Acta Crystallographica Section D
Biological Crystallography
ISSN 0907-4449

Multiple crystal forms of the cell-wall invertase inhibitor from tobacco support high conformational rigidity over a broad pH range

Michael Hothorn and Klaus Scheffzek*

European Molecular Biology Laboratory, Meyerhofstrasse 1, 69117 Heidelberg, Germany

Correspondence e-mail: scheffzek@embl.de

Received 3 February 2006
Accepted 30 March 2006

PDB References: Nt-CIF, pH 4.6, 2cj4, r2cj4sf; pH 5.0, 2cj5, r2cj5sf; pH 7.0, 1rj1, r1rj1sf; pH 7.0, $CdCl_2$, 1rj4, r1rj4sf; pH 7.5, 2cj6, r2cj6sf; pH 9.0, 2cj7, r2cj7sf; pH 9.5, 2cj8, r2cj8sf.

Plant acid invertases catalyse the breakdown of sucrose. Their activity is tightly regulated through interaction with specific protein inhibitors. The complex between the cell-wall invertase inhibitor Nt-CIF and its target enzyme is stable only at acidic pH, as found in the plant cell wall. Since the pH in this compartment can be modulated between pH 4 and 6 *in planta*, the rapid dissociation of the inhibitor–enzyme complex at neutral pH may represent a regulatory event. Here, it is analyzed whether the inhibitory component undergoes structural rearrangements upon changes in the pH environment. Six crystal forms grown at pH 4.6–9.5 and diffracting up to 1.63 Å indicate only small structural changes in CIF. This suggests that complex dissociation at neutral pH is mediated either by rearrangements in the enzyme or by a complex pattern of surface charges in the inhibitor–enzyme binding interface.

1. Introduction

Plant acid invertases (EC 3.2.1.26) convert the transport sugar sucrose into its building blocks glucose and fructose. They play important roles in cellular processes such as sugar transport, carbohydrate signalling and stress response (Roitsch & Gonzalez, 2004). Hence, altered invertase activity has dramatic consequences on plant growth and development (Cheng *et al.*, 1996; Tang *et al.*, 1999; Goetz *et al.*, 2001). Invertase activity is tightly controlled at the post-translational level through interaction with specific protein inhibitors. Plant genome-sequencing projects have grouped invertase inhibitors (Rausch & Greiner, 2004) with inhibitors of pectin methylesterase (PMEIs; Giovane *et al.*, 2004), an enzyme that is involved in the control of pectin metabolism and is structurally unrelated to invertases. All inhibitors share a size of about 18 kDa, two strictly conserved disulfide bridges and only moderate sequence homology (about 20% sequence identity).

Protein inhibitors of invertases are targeted towards extracellular isoforms that reside in the plant vacuole or the cell-wall compartment (Rausch & Greiner, 2004). A representative member of the family, the invertase inhibitor Nt-CIF (*Nicotiana tabacum* cell-wall inhibitor of β-fructosidase; referred to as CIF hereafter) forms a 1:1 complex with its target enzyme under acidic conditions that dissociates at neutral pH. In the plant cell wall, the pH may range between 4 and 6. The enzymatic activity of cell-wall invertase is strongly

Table 1
Summary of crystallization and X-ray analysis.

Values in parentheses are for the highest shell. The crystallization of the pH 4.6 and pH 9.5 forms has been reported previously (Hothorn *et al.*, 2003).

	pH 4.6	pH 5.0	pH 7.0†	pH 7.0 $CdCl_2$†	pH 7.5	pH 9.0	pH 9.5
Crystallization							
Precipitant	17% PEG 4K	19% PEG 4K	4.0 *M* Na formate	4.0 *M* Na formate	18% PEG 4K	18% PEG 4K	18% PEG 4K
Buffer	0.1 *M* NaOAc pH 4.0	0.1 *M* NaOAc pH 5.0	0.1 *M* bis-tris pH 7.0	0.1 *M* bis-tris pH 7.0	0.1 *M* bis-tris pH 7.5	0.1 *M* Tris pH 9.0	0.1 *M* Tricine pH 9.5
Salt	0.2 *M* Li_2SO_4	0.2 *M* Li_2SO_4		0.03 *M* $CdCl_2$	0.2 *M* NaI	0.2 *M* NaI	0.2 *M* NaI
Cryoprotectant	5%(*v*/*v*) glycerol	5%(*v*/*v*) glycerol	10%(*v*/*v*) glycerol	10%(*v*/*v*) glycerol	10%(*v*/*v*) glycerol	10%(*v*/*v*) glycerol	10%(*v*/*v*) glycerol
Data collection							
Beamline	ESRF, ID29	ESRF, ID14-4	ESRF, ID14-2	ESRF, ID14-2	DESY, BW7A	ESRF, ID14-4	DESY, BW7A
Detector	ADSC Q210 2D	ADSC Q4R CCD	ADSC Q4R CCD	ADSC Q4R CCD	MAR 165 mm CCD	ADSC Q4R CCD	MAR 165 mm CCD
Wavelength (Å)	0.9774	0.98	0.93	0.934	0.976	0.98	0.976
Data collection							
Space group	$P2_12_12$	$P6_322$	$C222_1$	$P2_12_12_1$	$P6_5$	$C222_1$	$P2_12_12_1$
Unit-cell parameters (Å)							
a	131.35	131.84	60.7	59.20	93.83	59.69	40.05
b	47.18	131.84	106.4	95.6	93.83	107.43	50.22
c	57.45	47.59	55.8	126.2	36.63	56.32	31.38
Resolution (Å)	1.63	1.84	1.87	2.0	2.00	1.80	2.38
Highest shell (Å)	1.72–1.63	1.95–1.84	2.00–1.87	2.15–2.0	2.12–2.00	1.90–1.80	2.58–2.38
No. of unique reflections	43726 (5886)	21167 (2857)	15167 (2455)	49059 (9428)	12748 (2001)	16850 (2529)	11192 (2339)
Multiplicity	7.3 (5.3)	10.1 (6.5)	8.3 (5.3)	7.3 (7.1)	4.9 (4.9)	7.3 (7.1)	7.1 (7.2)
$I/\sigma(I)$‡	11.7 (3.1)	15.4 (3.1)	23.8 (8.92)	16.1 (7.7)	7.8 (2.5)	14.3 (2.7)	13.6 (4.4)
R_{sym}‡ (%)	12.2 (49.0)	12.3 (65.1)	5.7 (12.7)	8.1 (25.8)	19.6 (65.1)	10.8 (72.4)	12.3 (45.3)
Completeness (%)	95.7 (81.5)	97.1 (83.1)	97.8 (88.2)	100 (100)	99.7 (98.5)	97.1 (91.4)	100 (99.7)
No. of molecules in ASU	2	1	1	4	1	1	2
Solvent content (%)	55.4	66.8	56.3	55.9	57.4	56.0	39.9

† Hothorn, D'Angelo *et al.* (2004). The values are included to facilitate comparison. ‡ As defined in *XDS* (Kabsch, 1993).

pH-dependent, with a maximum at about pH 4 *in vitro* (Roitsch & Gonzalez, 2004). Invertase activity might therefore be controlled by the surrounding pH environment in the extracellular space both at the enzymatic level and through changes in the binding affinity for the invertase inhibitor.

We are interested in the regulation of plant invertases and in the target specificity of their respective inhibitors. As a first step, we have previously determined the crystal structure of CIF (Hothorn, D'Angelo *et al.*, 2004). The inhibitor folds into an asymmetric four-helix bundle preceded by a short α-helical hairpin motif. A hydrophobic interface between the hairpin and the bundle core suggested both structural modules to be tightly integrated (Hothorn, D'Angelo *et al.*, 2004). Surprisingly, we could identify the corresponding α-hairpin in a PME inhibitor as adopting several conformations, allowing the formation of monomers and dimers in solution (Hothorn, Wolf *et al.*, 2004). Site-directed mutants and protein chimeras between CIF and PMEI suggest the α-hairpin motif in PMEI to be important for recruitment/binding of pectin methylesterase. Interfering with the conformational flexibility of this module reduces the inhibitory power of PMEI (Hothorn, Wolf *et al.*, 2004).

While the compact fold and interface stabilization in CIF do not favour pH-induced changes, the related PME inhibitor indeed exists in several conformations. We hypothesize that pH-induced structural alterations in CIF allow this inhibitor to exist in a binding (acidic) and a non-binding (neutral or basic) form. Here, we test this idea by crystallizing CIF in seven different pH environments ranging from pH 4.6 to 9.5 and solving its structure in six crystal forms.

2. Materials and methods

2.1. Crystallization and data collection

CIF was expressed and purified as described in Hothorn *et al.* (2003) and dialysed against 10 m*M* HEPES pH 7.0, 150 m*M* NaCl. Crystals were grown at room temperature by vapour diffusion from hanging drops composed of equal volumes (typically 1 + 1 µl) of protein solution (at about 12 mg ml^{-1}) and crystallization buffer suspended over a reservoir containing 0.5 ml crystallization buffer. Crystallization conditions for six crystal forms (Table 1; Hothorn *et al.*, 2003) were obtained using Crystal Screen, Crystal Screen 2 and PEG/Ion Screen (Hampton Research). Subsequently, conditions were refined by first adjusting the pH and then the concentration of precipitant. Crystals of different morphologies (Hothorn *et al.*, 2003) appeared overnight and grew to their final size within a few days. Crystals were transferred to reservoir solution containing 5–10%(*v*/*v*) glycerol, which served as cryoprotectant for all crystal forms described (Table 1).

Diffraction data were collected with the rotation method under cryogenic conditions and using monochromatic synchrotron radiation (Table 1). Complete data sets were recorded with high-resolution limits ranging from 2.38 to 1.63 Å (Table 1). The program *XDS* (Kabsch, 1993; June 2005 version) was used for data indexing, processing and scaling.

2.2. Structure solution and refinement

The molecular-replacement method as implemented in *Phaser* (McCoy *et al.*, 2005) was used to determine the structure of CIF in all crystal forms, using the previously

Table 2
Crystallographic refinement and geometry.

Values in parentheses are for the highest shell.

	pH 4.6	pH 5.0	pH 7.0†	pH 7.0 $CdCl_2$†	pH 7.5	pH 9.0	pH 9.5
Resolution range (Å)	19.65–1.63	43.94–1.84	19.25–1.87	19.67–2.00	46.93–2.00	38.87–1.80	19.21–2.38
Highest shell (Å)	1.67–1.63	1.88–1.84	2.00–1.87	2.13–2.00	2.05–2.00	1.85–1.80	2.44–2.38
No. of reflections	41534 (2217)	20107 (977)	15112 (2034)	49095 (7675)	12109 (875)	15920 (1058)	10602 (740)
R_{cryst}‡	0.151 (0.166)	0.180 (0.232)	0.194 (0.215)	0.212 (0.235)	0.217 (0.256)	0.185 (0.244)	0.197 (0.223)
R_{free}‡ (5% test set)	0.189 (0.228)	0.218 (0.256)	0.233 (0.238)	0.255 (0.275)	0.274 (0.286)	0.225 (0.289)	0.277 (0.319)
No. of atoms							
Protein	2216	1103	1107	4338	1107	1090	2140
Water	340	158	122	236	107	104	50
Ligand	31	22		72			
R.m.s. deviations							
Bond length (Å)	0.019	0.014	0.012	0.014	0.017	0.017	0.017
Angles (Å)	1.50	1.42	1.5	1.5	1.477	1.50	1.55
Mean *B* factor by atom type (Å^2)							
Protein	11.4	27.5	19.9	35.0	15.2	19.1	34.3
Water	17.7	32.9	31.2	36.7	27.9	36.4	31.6
Ligand	28.2	48.6		30.8	29.8	22.97	36.8
Ramachandran plot§							
Favoured (%)	93.4	91.5	93.1	93.2	93.8	93.7	92.2
Allowed (%)	6.6	7.7	6.1	6.6	6.2	6.3	7.0
Generously allowed (%)	0	0	0.8	0	0	0	0.4
Disallowed (%)	0	0.8	0	0.2	0	0	0.4
PDB code	2cj4	2cj5	1rj1	1rj4	2cj6	2cj7	2cj8

† Hothorn, D'Angelo *et al.* (2004). The values are included to facilitate comparison. ‡ As defined in *REFMAC*5 (Murshudov *et al.*, 1997). § As calculated in *PROCHECK* (Laskowski *et al.*, 1993).

determined CIF monomer (PDB code 1rj1; Hothorn, D'Angelo *et al.*, 2004) as a search model. The fast rotation and translation functions were calculated using data between 15 and 3.3 Å resolution. The resulting solutions were input into *ARP*/*wARP* v.6.1 (Morris *et al.*, 2003) for automated model building. Addition of sulfates, acetates (pH 4.6, 5.0) and iodines (pH 7.5, 9.0, 9.5) was followed by manual rebuilding in *COOT* (Emsley & Cowtan, 2004). All structures were refined using restrained TLS refinement as implemented in *REFMAC*5 (Murshudov *et al.*, 1997). Water molecules were added using *ARP_WATERS* and the occupancy of iodines was manually adjusted based on difference map analysis. Inspection of the refined models with *PROCHECK* (Laskowski *et al.*, 1993) revealed excellent stereochemistry (Table 2). Structural superpositions were calculated in *COOT* (Emsley & Cowtan, 2004).

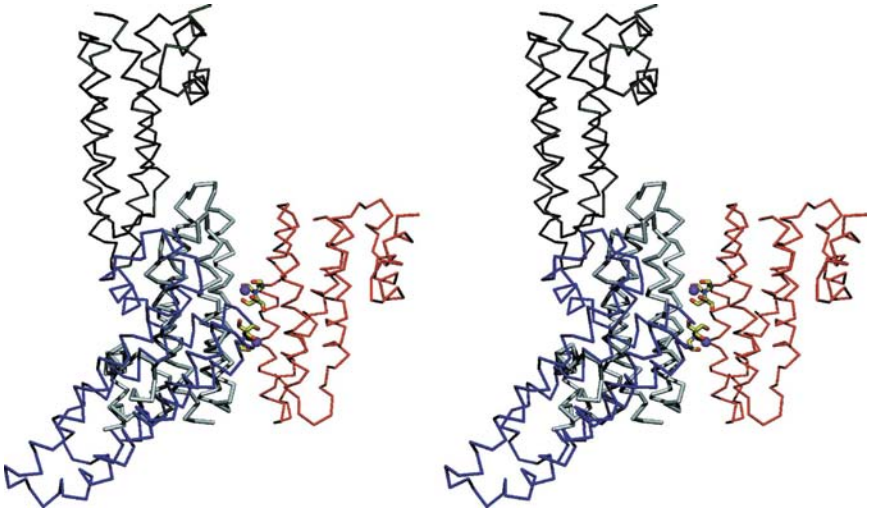

Figure 1
Lattice formation in CIF crystals involves different surfaces areas. Stereoview of the four molecules in the asymmetric unit of a primitive orthorhombic crystal form grown at pH 7.0 (PDB code 1rj4) depicted as C^{α} traces. Note that residues from distinct parts of the molecule, *e.g.* the longer core helices α5 and α6 (grey *versus* red molecule), the α-hairpin motif (grey *versus* blue molecule) and the loop regions (grey *versus* green molecule) establish crystallographic contacts. In addition, two Cd^{2+} ions (in magenta) and two Bis-Tris buffer molecules (in yellow) are involved in interface stabilization. The figure was prepared with *POVSCRIPT* (Fenn *et al.*, 2003) and *POV-Ray* (http://www.povray.org).

2.3. Crystal packing and conformational analysis

Symmetry-generated intermolecular contacts were determined with the program *CONTACT* using a distance cutoff between 2.1 and 3.2 Å. The corresponding surface areas were calculated with *AREAIMOL* (Collaborative Computational Project, Number 4, 1994).

Conformationally invariant and flexible regions in CIF were identified by least-squares superposition as implemented in *ESCET* (Schneider, 2002). Using 12 molecules from seven crystalline environments, highly similar conformers (with matrix elements larger than 0.98 in *ESCET*) were reduced to one representative with the minimal experimental error (mean e.s.d. in *ESCET*). The six remaining conformers were used for *ESCET* analysis.

3. Results and discussion

Purified CIF shares its N- and C-terminus with the mature inhibitor *in planta* (residues 20–166). The inhibitor crystallized in three initial conditions (Hothorn *et al.*, 2003). Two crystal forms at pH 7.0 were obtained using sodium formate as precipitant (Hothorn *et al.*, 2003; see Table 1). Based on PEG 4000 and Li_2SO_4, two novel crystal forms grew at pH 4.6 and 5.0, respectively (Table 1). Finally, adjusting the buffer conditions in the third initial hit (PEG 4000, NaI), three additional crystal forms covering pH 7.5–9.5 could be derived. Crystals diffracted to resolutions considerably better than 2.5 Å (Table 1). Currently, the best model of CIF has been refined at pH 4.6 from data collected at 1.63 Å resolution (Table 2).

3.1. Lattice packing analysis

Detailed crystal-packing analysis of the six independent crystal forms indicates that distinct surface areas of the inhibitor can be engaged in lattice formation. This is best illustrated by the arrangement of CIF molecules in a primitive orthorhombic crystal form grown at pH 7.0 (PDB code 1rj4; see Table 1; Hothorn, D'Angelo *et al.*, 2004). In this case, the asymmetric unit comprises four similar molecules (largest r.m.s.d. is ∼0.7 Å comparing 146 corresponding C^{α} atoms) that pack into crystallographic dimers either with a neighbouring or with a symmetry-related molecule. The core helices α5 and α6 (grey and red molecules in Fig. 1) mainly contribute to dimer formation along with two molecules of Bis-Tris buffer and two Cd^{2+} ions from the crystallization solution (Hothorn, D'Angelo *et al.*, 2004). The lattice is completed by the crystallographic dimers interacting with their hairpin motifs (shown in blue in Fig. 1) and the bundle-top loops (residues 60–67 and 119–126 in CIF; shown in green in Fig. 1). Notably, the contribution of the loop region 119–126 causes this loop to occur in several conformations (see below).

Hence, not all surface areas in CIF contribute to crystal packing in all crystal forms, as illustrated by a comparison of two CIF species grown at pH 7.0 (PDB code 1rj1; space group $C222_1$) and pH 5.0 (PDB code 2cj5; space group $P6_322$). Both crystal forms contain one molecule in their asymmetric units (Table 1), which superimpose with an r.m.s.d of ∼0.73 Å comparing 145 corresponding C^{α} atoms. The total surface area of CIF is 7900 $Å^2$ and about 2400 $Å^2$ is involved in crystal packing both at pH 5.0 and at pH 7.0, as calculated with the program *AREAIMOL*. However, only a third of this portion is involved in lattice stabilization in both crystal forms (Fig. 2). Moreover, analysis using *CONTACT* (see §1) indicates that none of the ionic interactions contributing to lattice formation are conserved among pH 5.0 and pH 7.0 crystals, possibly owing to the different pH environment.

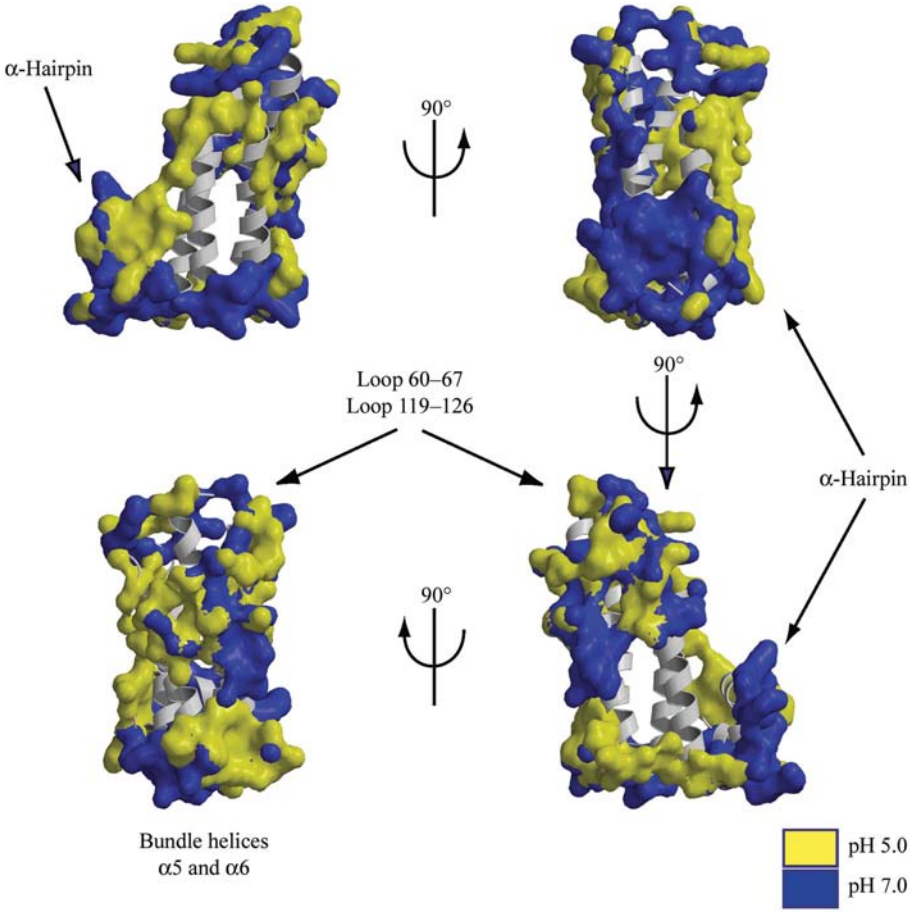

Figure 2
Large surface areas are involved in lattice formation in crystal forms grown at pH 5.0 and pH 7.0, respectively. CIF in ribbon representation (in grey) is shown in four different orientations together with surface patches involved in lattice formation at pH 5.0 (in yellow; PDB code 2cj5) and pH 7.0 (in blue; PDB code 1rj1). About a third of the packing surface area is common to crystals grown at pH 5.0 and pH 7.0, respectively. The surface areas were calculated with *AREAIMOL* (Collaborative Computational Project, Number 4, 1994). The figure was prepared using *POVSCRIPT* (Fenn *et al.*, 2003) and *GRASP* (Nicholls *et al.*, 1991).

3.2. Conformationally flexible and invariant parts in CIF

A structural comparison of all 12 molecules from seven crystalline environments (Table 1) did not reveal large rearrangements in CIF (the largest r.m.s.d. over all molecules and all corresponding C^{α} atoms is ∼0.8 Å). Detailed analysis in *ESCET* (Schneider, 2002), however, indicates that distinct parts of the inhibitor show different degrees of conformational flexibility. The most rigid part appears to be formed by the two longer N-terminal helices of the asymmetric four-helix bundle. Only small variations can be assigned to the short C-terminal helix pair of the four-helix bundle and to the

α-hairpin module itself. In this respect, it is noteworthy that both the four-helix bundle and the α-helical hairpin motif are stabilized by disulfide bonds and that high structural stability of CIF has been derived from its high melting temperature ($T_m \simeq 343$ K) in thermal unfolding experiments (Hothorn, D'Angelo *et al.*, 2004). The more flexible parts of the CIF structure appear to be located in loop regions connecting the bundle helices as well as in the small linker helix that joins the α-hairpin module and bundle core (Fig. 3).

The largest structural deviations occur in the longest loop (residues 119–126), which connects the shorter C-terminal helices of the four-helix bundle (Fig. 3). Since several conformations of this loop have also been observed in CIF crystals grown at pH 7.0 (see above), these variations cannot be attributed to changes in the surrounding pH environment. Moreover, the substitution of two solvent-exposed lysine residues in the loop by alanine residues has no significant effect on invertase activity in inhibition assays (S. Wolf & S. Greiner, personal communication).

While no large pH-induced changes could be identified in CIF, alterations in pH could be used to obtain a large number of lattice-packing arrangements starting from a minimal set of manually screened conditions. Therefore, the invertase inhibitor might prove to be a convenient tool for methodical studies, where many independent and decently diffracting crystal forms are desirable.

3.3. Implications for complex formation and pH-induced dissociation

In sharp contrast to the crystallographic analysis of the related PME inhibitor (Hothorn, Wolf *et al.*, 2004), we cannot identify large structural rearrangements in CIF. We have previously shown that conformational flexibility of the α-hairpin in PMEI is important for dimer formation (Hothorn, Wolf *et al.*, 2004). The lack of detectable hairpin flexibility in CIF is consistent with the monomeric behaviour of both the recombinant and plant-extracted inhibitor in size-exclusion chromatography (Weil *et al.*, 1994; Hothorn, Wolf *et al.*, 2004).

Our analysis highlights that the α-hairpin and four-helix bundle modules in CIF are tightly integrated and that pH-dependent formation of the enzyme–inhibitor complex is not controlled by large structural rearrangements in the inhibitory component. Instead, pH-induced changes might occur in the enzyme component itself. However, the most likely scenario is that CIF and its target enzyme use a rather charged interface for complex formation and that this interface contains residues that titrate in the pH range of interest.

The recent expression and crystallization of a cell-wall invertase from *Arabidopsis thaliana* (Verhaest *et al.*, 2005) and the identification of novel invertase inhibitors in the same organism (Link *et al.*, 2004) set the stage for crystallizing the enzyme–inhibitor complex. A high-resolution crystal structure of an invertase–CIF complex in concert with the biochemical analysis of mutant proteins will provide a more profound understanding of how CIF specifically inactivates cell-wall invertase. Finally, comparing the binding mode of CIF with that of a PME inhibitor in the PME–PMEI complex (DiMatteo *et al.*, 2005) should provide insight into how the puzzling target specificity of these related inhibitors is implemented on the structural level.

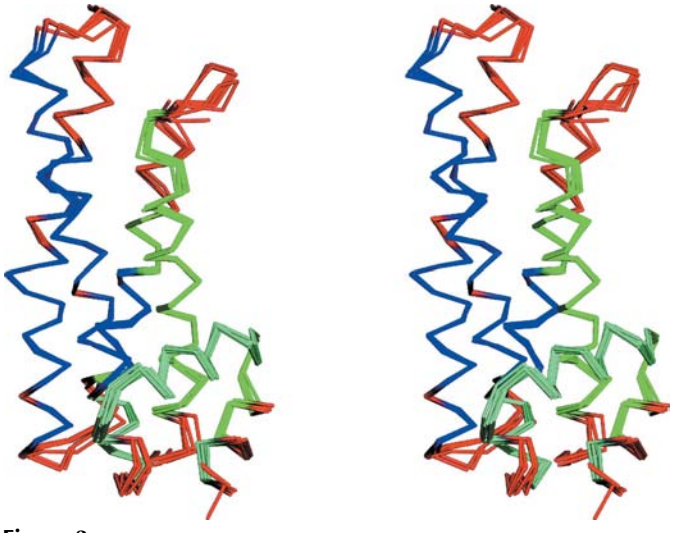

Figure 3
Conformationally flexible and invariant parts in CIF. Stereoview of six representative and superimposed conformers depicted as C^{α} traces. Parts identified as conformationally invariant are shown in blue, while more flexible parts are shown in red. The figure was prepared using *ESCET* (Schneider, 2002) and *PyMOL* (http://www.pymol.org).

We thank Esben Lorentzen for pointing out the *ESCET* program, Sebastian Wolf for biochemical analysis of mutant proteins, Steffen Greiner for discussion and the staff at beamlines ID14-4 and ID29 of the European Synchrotron Radiation Facility (ESRF), Grenoble, France and beamline BW7A, EMBL c/o DESY, Hamburg, Germany for technical support during data collection. MH gratefully acknowledges financial support from the Peter and Traudl Engelhorn Foundation, Penzberg, Germany.

References

Cheng, W. H., Taliercio, E. W. & Chourey, P. S. (1996). *Plant Cell*, **8**, 971–983.
Collaborative Computational Project, Number 4 (1994). *Acta Cryst.* D**50**, 760–763.
Di Matteo, A., Giovane, A., Raiola, A., Camardella, L., Bonivento, D., De Lorenzo, G., Cervone, F., Bellincampi, D. & Tsernoglou, D. (2005). *Plant Cell*, **17**, 849–58.
Emsley, P. & Cowtan, K. (2004). *Acta Cryst.* D**60**, 2126–2132.
Fenn, T. D., Ringe, D. & Petsko, G. A. (2003). *J. Appl. Cryst.* **36**, 944–947.
Giovane, A., Servillo, L., Balestrieri, C., Raiola, A., D'Avino, R., Tamburrini, M., Ciardiello, M. A. & Camardella, L. (2004). *Biochim. Biophys. Acta*, **1696**, 245–252.
Goetz, M., Godt, D. E., Guivarc'h, A., Kahmann, U., Chriqui, D. & Roitsch, T. (2001). *Proc. Natl Acad. Sci. USA*, **98**, 6522–6527.
Hothorn, M., Bonneau, F., Stier, G., Greiner, S. & Scheffzek, K. (2003). *Acta Cryst.* D**59**, 2279–2282.
Hothorn, M., D'Angelo, I., Marquez, J. A., Greiner, S. & Scheffzek, K. (2004). *J. Mol. Biol.* **335**, 987–995.

Hothorn, M., Wolf, S., Aloy, P., Greiner, S. & Scheffzek, K. (2004). *Plant Cell*, **16**, 3437–3447.
Kabsch, W. (1993). *J. Appl. Cryst.* **26**, 795–800.
Laskowski, R. A., MacArthur, M. W., Moss, D. S. & Thornton, J. M. (1993). *J. Appl. Cryst.* **26**, 283–291.
Link, M., Rausch, T. & Greiner, S. (2004). *FEBS Lett.* **573**, 105–109.
McCoy, A. J., Grosse-Kunstleve, R. W., Storoni, L. C. & Read, R. J. (2005). *Acta Cryst.* D**61**, 458–464.
Morris, R. J., Perrakis, A. & Lamzin, V. S. (2003). *Methods Enzymol.* **374**, 229–244.
Murshudov, G. N., Vagin, A. A. & Dodson, E. J. (1997). *Acta Cryst.* D**53**, 240–255.
Nicholls, A., Sharp, K. A. & Honig, B. (1991). *Proteins*, **11**, 281–296.
Rausch, T. & Greiner, S. (2004). *Biochim. Biophys. Acta*, **1696**, 253–261.
Roitsch, T. & Gonzalez, M. C. (2004). *Trends Plant Sci.* **9**, 606–613.
Schneider, T. R. (2002). *Acta Cryst.* D**58**, 195–208.
Tang, G. Q., Luscher, M. & Sturm, A. (1999). *Plant Cell*, **11**, 177–189.
Verhaest, M., Le Roy, K., Sansen, S., De Coninck, B., Lammens, W., De Ranter, C. J., Van Laere, A., Van den Ende, W. & Rabijns, A. (2005). *Acta Cryst.* F**61**, 766–768.
Weil, M., Krausgrill, S., Schuster, A. & Rausch, T. (1994). *Planta*, **193**, 438–445.